Atmósfera 38, 759-778 (2024)
https://doi.org/10.20937/ATM.53356

Simulation of the Planetary Boundary Layer characteristics and its relation to air quality in the Metropolitan Area of Rio de Janeiro, Brazil

Wilson William DA SILVEIRA[1], Vanessa Silveira Barreto CARVALHO[1]*, Aline Araújo DE FREITAS[1], Michelle Simões REBOITA[1] and Taciana Toledo de Almeida ALBUQUERQUE[2]

[1] *Instituto de Recursos Naturais, Universidade Federal de Itajubá, Itajubá, 37500076, Minas Gerais, Brazil.*
[2] *Departamento de Engenharia e Sanitária Ambiental, Universidade Federal de Minas Gerais, Belo Horizonte, 31270010, Minas Gerais, Brazil.*
*Corresponding author; email: vanessa.silveira@unifei.edu.br

Received: November 14, 2023; Accepted: April 2, 2024

RESUMEN

En la Región Metropolitana de Río de Janeiro (RMRJ), las estaciones de monitoreo de la calidad del aire registran con frecuencia concentraciones de partículas en suspensión (PM_{10}) y ozono (O_3) superiores a los valores de referencia propuestos por la Organización Mundial de la Salud. En esta región, las condiciones climáticas combinadas con altas emisiones de contaminantes atmosféricos y una topografía compleja favorecen la ocurrencia de altas concentraciones de contaminantes como PM_{10} y O_3 durante varios días consecutivos. Por lo tanto, este estudio evaluó (1) las condiciones de la capa límite planetaria (PBL, por su sigla en inglés) simuladas por el modelo WRF, y (b) su relación con la calidad del aire registrada durante los días con altas concentraciones de O_3 y PM_{10} en el MARJ. Se consideraron dos episodios, uno durante el verano cuando se registraron altas concentraciones de O_3 y otro durante el invierno con altas concentraciones de PM_{10}. El estudio utilizó el modelo de investigación y pronóstico del clima (WRF) para simular las condiciones durante dichos periodos. Se utilizaron observaciones de superficie y de la capa superior atmosférica, gráficos sinópticos e imágenes de satélite para verificar los resultados del WRF. En ambos periodos fue posible identificar la influencia del anticiclón subtropical del Atlántico Sur asociado a condiciones de cielo despejado, ligero subsidencia del aire y vientos más débiles. La comparación con las observaciones mostró que el modelo simuló con coherencia las condiciones climáticas. Los vientos más débiles y el comportamiento de la brisa marina durante la tarde favorecen el mantenimiento de los contaminantes y su transporte hacia el noreste/noroeste de la región. En general, el modelo WRF representó consistentemente la altura de la PBL y la estabilidad atmosférica. Por lo tanto, este estudio muestra que los resultados del WRF pueden usarse para simular condiciones de la PBL y podrían usarse como fuente de información de la capa superior del aire en el MARJ.

ABSTRACT

Frequently in the Metropolitan Area of Rio de Janeiro (MARJ), air quality monitoring stations record concentrations of particulate matter (PM_{10}) and ozone (O_3) above the reference values proposed by the World Health Organization. In this region, weather conditions combined with high atmospheric pollutant emissions and complex topography favor the occurrence of high concentrations of pollutants such as PM_{10} and O_3 for several consecutive days. Hence, this study evaluated 1) the Planetary Boundary Layer (PBL) conditions simulated by the Weather Research and Forecasting (WRF) model and b) its relation to the air quality recorded during days with high concentrations of O_3 and PM_{10} in the MARJ. Two episodes, one during summertime when high O_3 concentrations were registered and one during the winter with high PM_{10} concentrations, were considered. The study used the WRF model to simulate conditions during those periods. Upper air and surface observations, synoptic charts, and satellite images were used to verify WRF results. In both periods, it was possible to identify the influence of the South Atlantic Subtropical Anticyclone associated with clear sky

conditions, slight air subsidence, and weaker winds. The comparison with observations showed the model simulated coherently local weather conditions. Weaker winds and the performance of the sea breeze during the afternoon favored the maintenance of pollutants and their transport to the northeast/northwest of the region. In general, WRF consistently represented the height of the PBL and atmospheric stability. Therefore, this study shows that WRF results can be used to simulate PBL conditions and could be used as a source of upper air information in the MARJ.

Keywords: ozone, particulate matter, weather conditions, atmospheric stability, WRF.

1. Introduction

Megacities are regions with a population exceeding 10 million inhabitants (Muramatsu et al., 2021). According to the United Nations (UN, 2019), in 2018, about 6.9% of the world's population lived in megacities, and it is estimated that by 2030 this number will reach 8.8%. In South America, Brazil has two megacities: São Paulo, with an estimated population of 21.65 million inhabitants in 2018, and Rio de Janeiro, with 13.29 million inhabitants (UN, 2019; UN-HABITAT, 2022). The increase in the population living in these areas directly impacts air quality, which is also influenced by factors such as topography, meteorology, patterns associated with urban mobility, and emissions of different fuel types, among others (Baklanov et al., 2016; Molina, 2021; UN, 2022).

The megacity of Rio de Janeiro corresponds to the Metropolitan Area of Rio de Janeiro (MARJ), which comprises 21 municipalities, has the second largest vehicle fleet in the country with 3.1 million vehicles (Santos and Azevedo, 2021), and a high concentration of industries. It is estimated that vehicular sources are responsible for 77% of the total emissions of atmospheric pollutants in the region and industrial sources for 23% (INEA, 2020). In addition to the variability and exposure to emission sources, other factors, such as the complex topography of the region and the presence of large bodies of water, such as Baía de Guanabara, can also significantly impact pollutant concentration values and reduce the scale of representativeness of air quality monitoring sites (Santos et al., 2016; da Silveira and Carvalho, 2021).

Air quality monitoring in the MARJ started in the late 1960s (Cavalcanti, 2003); however, even with the network's expansion from the 1990s onwards, the number of air quality monitoring sites is still insufficient when analyzing the territorial extension of the area. Nowadays, the Air Quality Monitoring Network of the Instituto Estadual do Ambiente (State Environment Institute, INEA) has 150 air quality and weather stations spread across the state of Rio de Janeiro (INEA, 2020).

Among air pollutants, high concentrations of particulate matter with a diameter of less than 10 μm (PM_{10}), and ozone (O_3) are frequently recorded in the MARJ (Santos et al., 2016; Dantas et al., 2020; Gómez-Peláez et al., 2020; Mendes et al., 2020; Moura et al., 2020; da Silveira and Carvalho, 2021). For the MARJ, several studies have shown that (a) in conditions of intense winds and high precipitation, pollutants such as PM_{10} and O_3 registered lower concentrations (Trindade et al., 1980; Carvalho et al., 2012; Santos et al., 2016; Beringui et al., 2023); (b) high temperatures and low values of relative humidity, absence of precipitation (and, consequently, clear skies), and light winds were associated with high O_3 concentrations (Carvalho et al., 2012; Geraldino et al., 2017; Silveira and Carvalho, 2021; Beringui et al., 2023); and, (c) when extended to the west, the South Atlantic Subtropical Anticyclone (SASA; Reboita et al., 2019) contributes with atmospheric stability over the southeast region of Brazil, which is characterized by light winds, low cloudiness and, consequently, absence of precipitation. Under this scenario, there is an increase in the concentration of pollutants throughout the southeast region, as identified by da Silva Júnior and Andrade (2013), Carvalho et al. (2015), Santos et al. (2016), and da Silveira and Carvalho (2021).

Atmospheric stability is related to the Planetary Boundary Layer (PBL) features. It refers to the tendency of the air to resist vertical movements and it is a highly relevant factor to air quality since it directly influences the concentration of pollutants in the atmosphere. In stable atmospheric conditions, convection and turbulence are inhibited, leading to high concentrations of pollutants such as PM_{10} and O_3 precursors in the lower troposphere; in contrast,

unstable conditions, with intense buoyancy, convection, and air turbulence, favor the dispersion of pollutants in the atmosphere (Zhang et al., 2012; Crawford et al., 2016; Wang et al., 2016; Bodor et al., 2022).

It is important to emphasize that the association of atmospheric conditions and air pollution can be studied through numerical models. Li et al. (2019) showed the influence of stable conditions on the increase of surface pollutant concentrations in northeast China through a tracer simulation with the Weather Research and Forecasting (WRF) model with chemistry (WRF-Chem). A study in megacities in China also revealed that the induced thermodynamic perturbations and turbulent mixings associated with urbanization processes favor the growth of PBL and the dispersion of pollutants; however, these processes also increase air pollutants emissions, generally increasing aerosol concentrations (Miao et al., 2019).

The impact of the PBL structure on episodes with high concentrations of pollutants in the MARJ has been little explored in the literature. From the observational point of view, this is mainly due to the scarcity of upper air data in the region, where measurements are only carried out at Tom Jobim International Airport through radiosondes twice daily, at 00:00 and 12:00 UTC. Hence, numerical weather forecast models can complement the information obtained from local observations to identify patterns associated with high pollutant concentrations and improve air quality forecasts, even allowing the analysis of the PBL structure in regions without records. In this context, the main objectives of this study are to evaluate (1) the PBL conditions simulated by the WRF model and (b) its relation to the air quality registered during days with high concentrations of O_3 and PM_{10} in the MARJ.

2. Materials and methods

2.1. Study area and data

PM_{10} and O_3 concentrations data from eight sites located in Rio de Janeiro municipality were analyzed: (1) Copacabana, (2) São Cristóvão, (3) Centro, (4) Tijuca, (5) Irajá, (6) Bangu, (7) Campo Grande, and (8) Pedra de Guaratiba, as shown in Figure 1. The 10-minute concentration averages of PM_{10} and O_3 from 2012 to 2015 were used to select air quality episodes with high concentration values (section 2.2). Air temperature, relative humidity, wind direction, and wind speed obtained at these sites at the station level were also used. All data was made available by the Rio de Janeiro City Administration at http://www.data.rio/.

Precipitation data obtained from eight pluviometric stations located in the same neighborhoods as the air quality monitoring sites were obtained through the Rio de Janeiro City Alert System (alertario.rio.rj.gov.br). Cloud cover data from the METAR from Tom Jobim International Airport, available on the Air Force Command Meteorology Network website (REDEMET; www.redemet.aer.mil.br), and soundings data, available from the University of Wyoming website (weather.uwyo.edu/upperair/sounding.html) of the same airport were also considered. Synoptic charts provided by the Center for Weather Forecast and Climatic Studies of the National Institute for Space Research (CPTEC/INPE; http://tempo.cptec.inpe.br/) were also used to analyze large-scale meteorological conditions. Images from the GOES satellite were also used to assist in the cloud cover analysis.

2.2 Cases selection

To select the cases of study, the 8-h moving averages of O_3 concentrations and daily averages of PM_{10} were calculated. Then, the highest moving 8-h averages of O_3 concentrations per day and PM_{10} daily average concentrations were compared to the values established for the final phase of the National Air Quality Standard (PF) (100 μg m^{-3} for O_3 and 50 μg m^{-3} for PM_{10}) from Resolution 491 of the Conselho Nacional do Meio Ambiente (National Council for the Environment, CONAMA) (CONAMA, 2018). Notably, the first phase of the PFs (PI-1) is still in effect throughout most of the Brazilian states, with values of 140 μg m^{-3} for O_3 and 120 μg m^{-3} for $PM_{10,}$ and another two phases are intended before the implementation of the PF. We should highlight that CONAMA Resolution 491 considered, as a reference, the values proposed by the World Health Organization (WHO, 2005). However, in 2021, the WHO released a new update on these values (WHO, 2021), indicating even more restrictive concentrations as a reference for the protection of human well-being and health. Adopting more restrictive values is expected to reduce the number of deaths related to air pollution, which accounts for about seven million people annually (Carvalho, 2021).

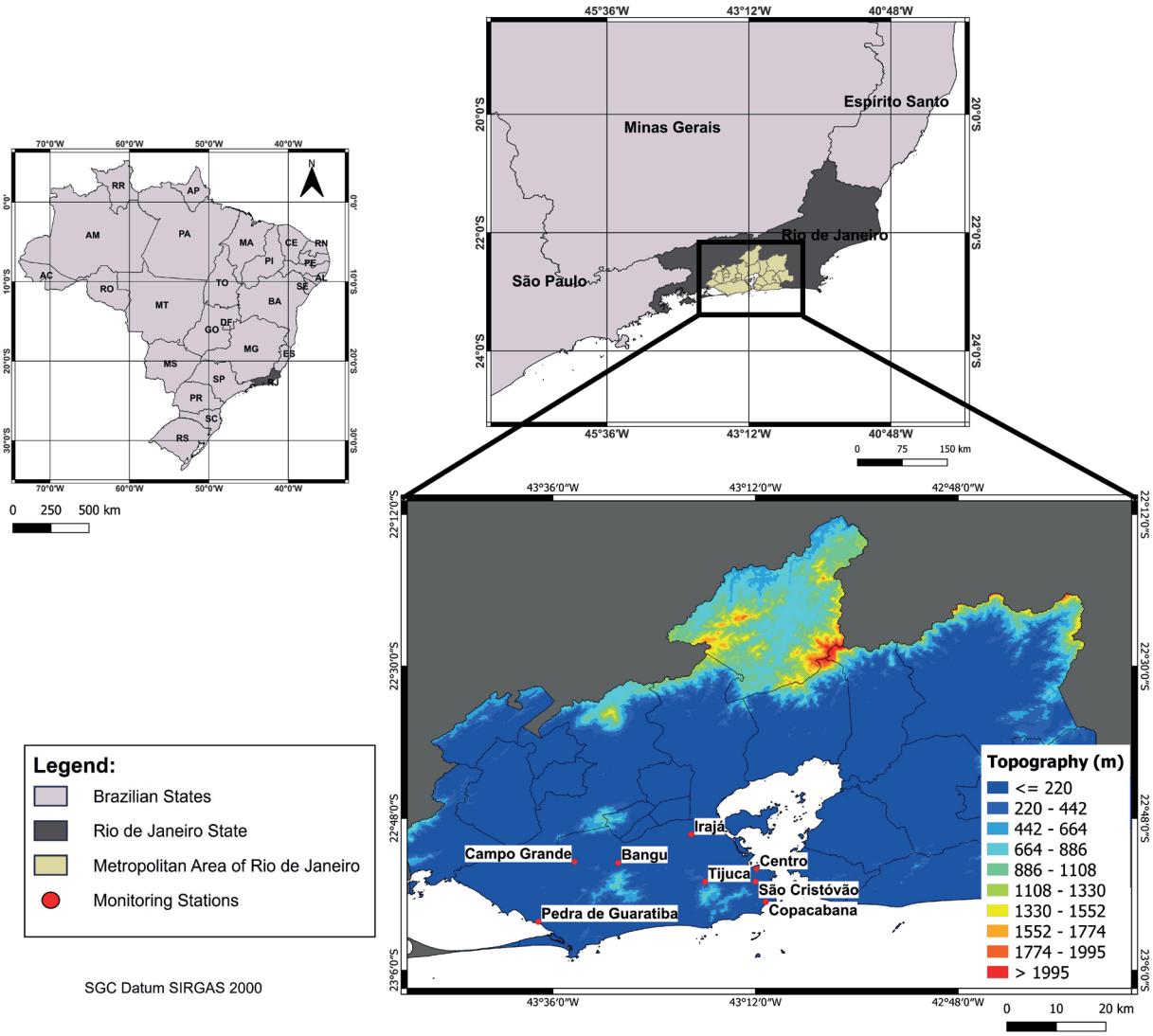

Fig. 1. Location of the Metropolitan Area of Rio de Janeiro (MARJ), Brazil, the spatial distribution of the air quality monitoring sites, and topography (m).

The criteria to define two cases of study, one for each pollutant, were that at least three of eight air quality monitoring sites had maximum averages higher than the reference values. A seven-day period when PM_{10} daily average concentrations were higher than 50 μg m^{-3} was selected during winter and a six-day period during the summer was selected when the maximum daily 8-h O_3 concentrations were higher than 100 μg m^{-3}. Winter and summer are when higher concentration levels of PM_{10} and O_3 are recorded in the MARJ, respectively (Carvalho, 2010; Santos et al., 2016; Tsuruta et al., 2018). The first period selected (P1), from August 1 to 7, 2013, during winter, showed daily mean concentrations of PM_{10} above 50 μg m^{-3} (Table I) in at least three sites under analysis during the study days. All sites recorded concentrations above the PF in four of the seven days. This shows how compromised the region is when it comes to PM_{10} concentrations. In four of the eight sites, concentration values were twice or even three times higher than 50 μg m^{-3} on specific days. For instance, the Irajá site, located in a residential neighborhood with more than 95 000 inhabitants and close to high vehicular traffic areas

Table I. Daily average concentrations of PM_{10} (μg m^{-3}) recorded in the Metropolitan Area of Rio de Janeiro (MARJ) from August 1 to 7, 2013 (P1).

Monitoring stations	August						
	1	2	3	4	5	6	7
Bangu	**64.13**	**56.78**	**80.07**	**60.35**	35.79	38.74	**60.88**
Centro	**75.96**	**100.79**	**96.33**	**65.58**	40.35	**50.83**	**71.13**
Campo Grande	**88.21**	**93.29**	**90.21**	**79.74**	47.04	**58.71**	**79.75**
Copacabana	**74.97**	**101.83**	**97.62**	**95.02**	**64.33**	**67.49**	**69.57**
Irajá	**108.00**	**169.26**	**131.96**	**89.13**	**50.57**	**70.25**	**75.91**
Pedra Guaratiba	**75.96**	**100.79**	**96.33**	**65.58**	40.35	**50.83**	**71.13**
São Cristóvão	**76.33**	**107.08**	**107.79**	**80.08**	**50.92**	**61.92**	**61.54**
Tijuca	**67.26**	**84.42**	**82.99**	47.22	42.00	**56.46**	**57.16**

Records above the reference values are highlighted in bold.

(Mello, 2017), registered a maximum concentration value of 169.26 μg m^{-3} on August 2.

Between January 21 and 26, 2014 (P2), during the austral summer, the 8-h maximum O_3 concentrations were above 100 μg m^{-3} in at least four stations under analysis during the study days (Table II). As identified for P1, at some point all stations considered presented values higher than those recommended for the final phase of CONAMA's Resolution 491 (CONAMA, 2018).

2.3. Model configurations

Simulations were performed with the WRF model for the two selected periods, with the following objectives: (a) to verify the performance of the model in simulating the conditions of atmospheric stability (since there is a high concentration of pollutants, the hypothesis is that there are stable atmospheric conditions) and the meteorological variables and (b) to analyze their relation mainly in what refers to the influence of atmospheric stability in the concentrations of pollutants recorded in the region. It is worth noting that the WRF is an atmospheric modeling system that includes physical, dynamic, and computational equations and can be applied to weather forecasting, data assimilation studies, and coupled geophysical models (Skamarock et al., 2008).

The data for initialization and generation of initial and boundary conditions were obtained from the Global Forecast System (GFS) with 0.5º spatial horizontal resolution every 6 h through the National Climatic Data Center of the National Oceanic and

Table II. 8-h maximum O_3 concentrations, in μgm^{-3}, recorded at the MARJ from January 21 to 26, 2014 (P2).

Monitoring stations	January					
	21	22	23	24	25	26
Bangu	**147.85**	**121.49**	**168.83**	**155.14**	**154.29**	**118.94**
Centro	**123.58**	**124.80**	**152.75**	**132.80**	**144.69**	**115.78**
Campo Grande	84.82	77.21	70.40	87.98	**100.99**	89.76
Copacabana	38.44	43.58	50.02	38.32	56.99	38.94
Irajá	**105.10**	**105.82**	**142.24**	**112.57**	**165.91**	**144.14**
Pedra Guaratiba	**123.58**	**124.80**	**152.75**	**132.80**	**144.69**	**115.78**
São Cristóvão	62.74	65.79	73.60	57.07	82.07	69.81
Tijuca	—	—	**129.86**	83.96	**136.97**	**128.55**

Records above the reference values are highlighted in bold.

Atmospheric Administration website (NCDC/NOAA [nomads.ncdc.noaa.gov]). Three nested grids with a resolution of 27, 9, and 3 km (Fig. 2) and 33 vertical levels were considered. The grids were centered at 22.8º S and 43.25º W. All simulations were triggered 24 h before the period of interest to eliminate the spin-up effect of the model. A summary of the model settings can be seen in Table III. Results obtained from da Silveira and Carvalho (2021) were used to define the model settings in this study.

2.4. Analyses

The synoptic charts and the WRF results for the 27 km grid and the 3 km grid were used to evaluate the atmospheric patterns on a synoptic scale. The results obtained with the WRF model for the 3-km grid and the meteorological data observed in the region were used to analyze the prevailing meteorological conditions on a local scale.

Initially, we compared the large-scale pattern of the mean sea level pressure between synoptic charts and experiments. A comparison of the cloud coverage followed this analysis. The percentage of the sky covered by clouds was obtained from METAR data where CAVOK means Ceiling and visibility okay, SKC signifies Sky clear (clear below 12 000 for ASOS/AWOS), NSC denotes No significant clouds, FEW represents 1/8 to 2/8 of sky cover, SCT means Scattered with 3/8 to 4/8 of sky cover, BKN is Broken when the sky cover is from 5/8 to 7/8, and OVC indicates Overcast with 8/8 of sky cover (DECEA, 2023).

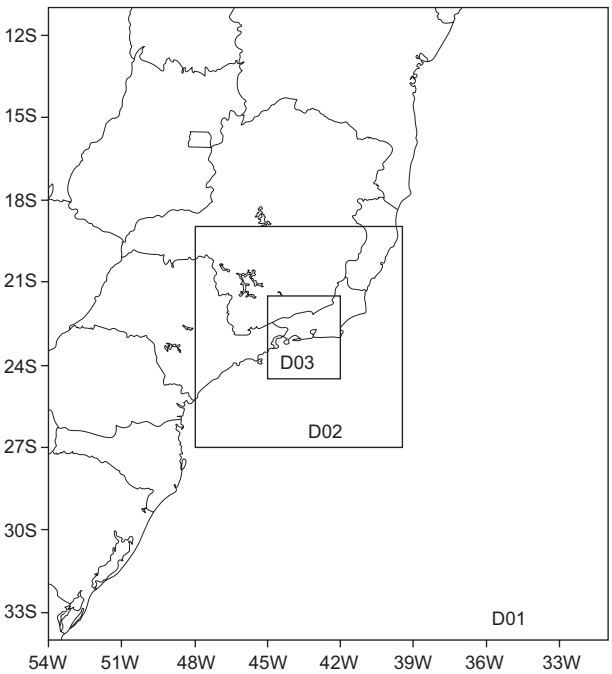

Fig. 2. WRF domain and nested grids.

The conditions of atmospheric stability, PBL height, and vertical profile of the atmosphere were determined. Wind roses were generated from the wind data recorded at the stations to verify the diurnal evolution of the sea breeze using the WRPLOT View software.

Table III. Model configuration and physical parameters.

Parameterization	Grid 1	Grid 2	Grid 3
Points in the *x* direction	95	97	94
Points in the *y* direction	95	97	94
Vertical levels	33	33	33
Horizontal resolution	27 km	9 km	3 km
Central latitude	22.80º S		
Central longitude	43.25º W		
Microphysics	Purdue-Lin (Chen and Sun, 2002)		
Cumulus	Kain-Fritsch (Kain, 2004)*		
Planetary boundary layer	YSU (Hong et al., 2006)		
Surface layer	Eta similarity (Janjić, 2001)		
Short wave radiation	Dudhia shortwave (Dudhia, 1989)		
Long wave radiation	RRTM (Mlawer et al., 1997)		

YSU: Yonsei University; RRTM: rapid radiative transfer model.
*Only enabled for grid 1.

The atmospheric stability classification was carried out by calculating the Richardson number (Eq. [1]) as proposed by Stull (1991) due to the Ri number presenting a good performance when compared to the other classification methods and data availability (Mohan and Siddiqui, 1998).

$$Ri = [g\ \theta v^{-1}][(\Delta\theta v\ \Delta z^{-1})\ ((\Delta u\ \Delta z^{-1})^2)^{-1} \quad (1)$$

where g is the acceleration of gravity (9.8 m s^{-2}), Δz (m) is the variation in height, Δu (m s^{-1}) is the variation in wind speed, θv (K) is the average temperature virtual potential between the two levels and the term $\Delta\theta v\ \Delta z^{-1}$ is the difference in the virtual potential temperature along the vertical.

Calculations of the parameters required for determining the atmospheric stability were performed for the PBL using the data obtained from the upper air soundings. The classification proposed by Clifton et al. (2013) was used: (a) unstable when $Ri < -0.01$; (b) neutral when $-0.01 < Ri < 0.01$, and (c) stable when $Ri > 0.01$.

The PBL height was determined through the visual method using the vertical profile of the potential temperature for the 12:00 UTC upper air soundings. For 00:00 UTC upper air soundings, specific humidity data were also used to determine the extent of the PBL, as proposed by Sánchez (2017), since the vertical profile of potential temperature was almost constant throughout the troposphere. The atmospheric stability simulated was classified through the methodology proposed by Clifton et al. (2013), analogous to the classification made from the observations. The vertical extent of the PBL can be characterized by a layer where the potential temperature and specific humidity are constant. In these cases, the PBL height can be identified as the height where the potential temperature and specific humidity present an abrupt increase and decrease, respectively (Sánchez, 2017),

3. Results and discussions

3.1. Atmospheric conditions of the selected case studies

3.1.1 Mean sea level pressure

Considering the two study cases (from August 1 to 7, 2013 [P1] and from January 21 to 26, 2014 [P2]), the visual comparison between the sea level pressure simulated by the WRF model through the course domain (27 km) and the synoptic chart shows an agreement in simulating the configuration of the high-pressure system in both periods (as an example, see Fig. 3). The climatological configuration of the SASA during the winter is its expansion over southeastern Brazil, and during summer its retraction eastward, leaving the Brazilian area. But, in anomalous situations, the SASA can also expand westward during summer, influencing southeastern Brazil (Reboita et al., 2010; Ferreira and Reboita, 2022). Figure 3 shows that the SASA configuration is more pronounced during winter, a fact verified by the synoptic charts and the model results. In the case study of summer, SASA is showing an anomalous configuration, which should contribute to the pollutant concentration as in Carvalho et al. (2012), da Silva Junior and Andrade (2013), Santos et al. (2016), and da Silveira and Carvalho (2021).

3.1.2 Cloud cover

METAR data shows that the percentage of hours with cloud coverage $\leq 2/8$ was greater than 69% for P1 and 95% for P2 (Fig. 4). No precipitation was recorded at the eight sites during P1. During P2, there were records of light precipitation in the following stations: Irajá: 2.4 mm on January 22 at 16:00 LT; Bangu: 3.2 mm on January 24 at 21:00 LT; and Campo Grande: 0.4 mm on January 24 at 20:00 LT. Despite the Irajá station recording precipitation values during the afternoon, a favorable time for the formation of O_3, no significant drop in concentrations was verified; on the contrary, values above the threshold established for comparison were registered. This is probably due to the low precipitation (insufficient to remove precursors) and the low cloud cover during most of the day.

When compared to METAR data, WRF results for the 3-km grid revealed that the model can satisfactorily represent the cloud cover in the study area, indicating a predominance of clear skies in both periods. As an example, Figure 5a shows, through the 15Z satellite image of August 3, 2013, the predominance of clear skies under RMRJ; the same is verified in Figure 5c through the cloud cover simulated by the model during the first period. Similarly, the 12Z satellite image of January 26, 2014 (Fig. 5b) during the second period, exemplifies the low cloud cover condition over the area and its respective representation through the WRF (Fig. 5d).

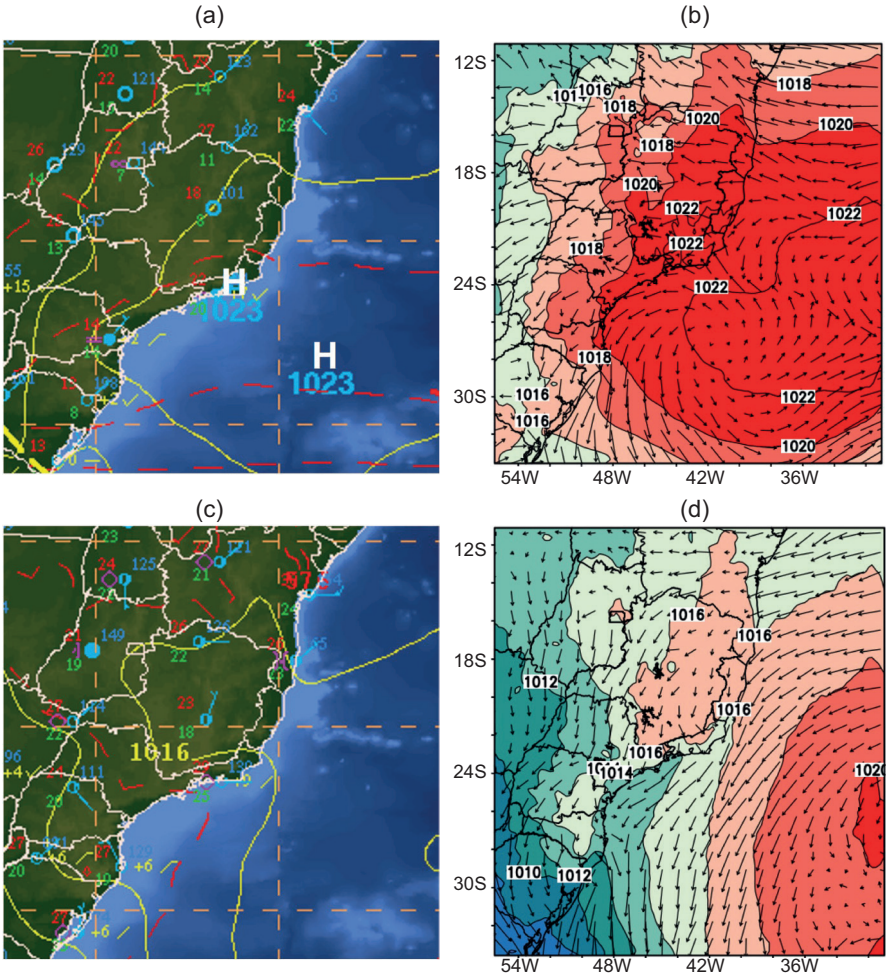

Fig. 3. Synoptic charts of (a) 06/08/2013 at 00:00 UTC and (c) 21/01/2014 at 12:00 UTC, where the yellow lines are the isobars and the blue symbols present the surface synoptic observations (SYNOP). Mean sea level pressure (hPa) and wind (m s^{-1}) simulated by the WRF (27-km grid) of (b) 06/08/2013 at 00:00 UTC and (d) 01/21/2014 at 12:00 UTC, where the arrows indicate wind direction and speed.

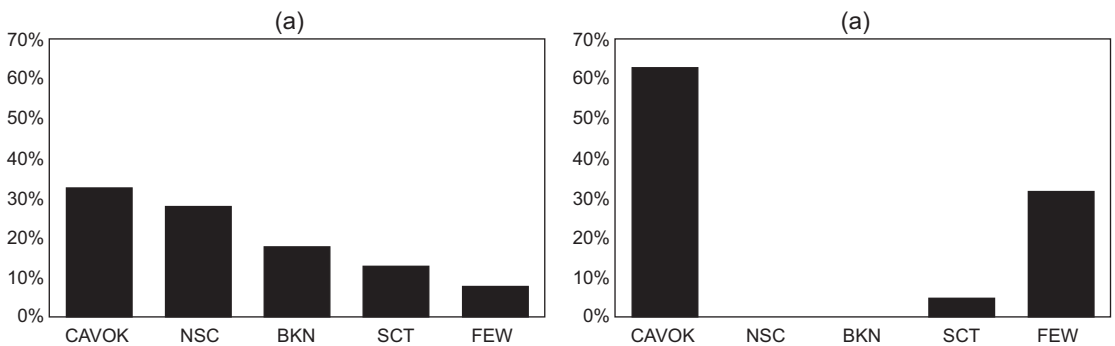

Fig. 4. Frequency of occurrence of cloud cover classes used daily in METAR messages. (a) In the period from 08/01/2013 to 08/07/2013 and (b) from 01/21/2014 to 01/26/2014 at the Galeão Airport (SBGL).

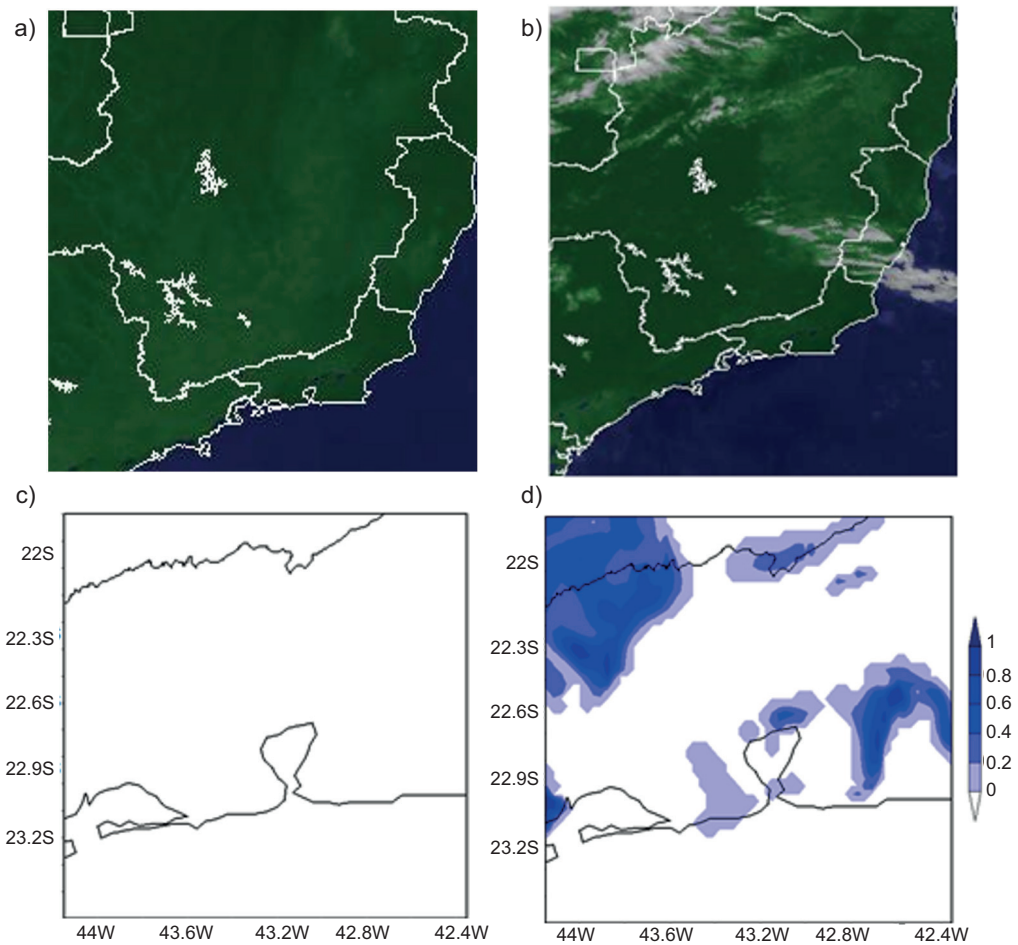

Fig. 5. GOES satellite images (in color) of (a) August 3, 2013 (15:00 UTC) and (b) February 10, 2014 (12:00 UTC). Cloud cover (%) through the 3-km grid (WRF) on (c) August 3, 2013 (15:00 UTC) and (d) January 26, 2014 (14:00 UTC).

It is important to highlight that the absence of precipitation during most days in P1 contributed to high concentrations of PM_{10} on successive days since it prevents the removal of the pollutant and favors its accumulation. In P2, the predominance of high visibility levels, which implies low or absent cloud cover, favors the formation of O_3 since this process depends on the incidence of solar radiation; in contrast, the absence of precipitation hinders the removal of precursors in the atmosphere, favoring their accumulation. Since most of the precipitation recorded during P2 occurred during the night, mostly associated with cloud cover between 1/8 to 2/8 (probably due to the local convection process), it seems not to impact O_3 formation in the area. These results agree with those obtained by Santos et al. (2016) for particulate matter and by Carvalho et al. (2015) and Schüch et al. (2019) for O_3.

3.1.3 Winds at 10 m

The wind roses for the closest ocean station, Pedra de Guaratiba, exemplify the action of the sea breeze on the region's coast during the afternoon, when it is more intense (Fig. 6). For both periods (P1 and P2), more intense winds were observed coming from the southwest, a direction typically associated with sea breezes in this area of the MARJ (Dereczynski et al., 2009; Pimentel et al., 2014), which favors the transport of pollutants to regions located northeast of the region (Carvalho, 2010). Due to its location,

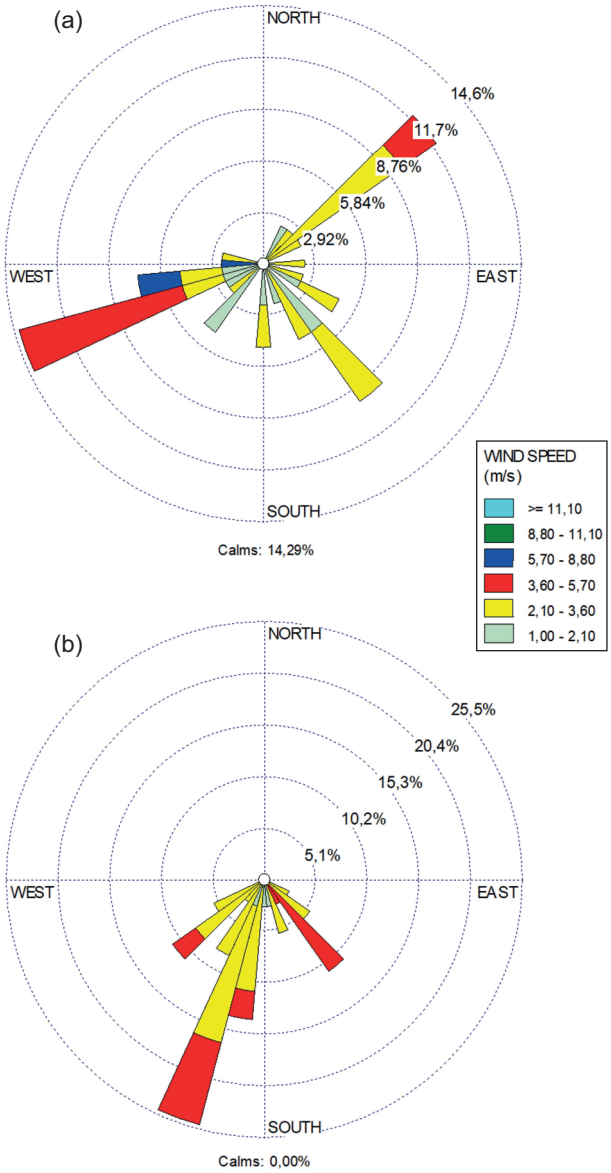

Fig. 6. Winds at 10 m registered between 13:00 and 18:00 LT at Pedra de Guaratiba station for the periods from (a) 08/01/2013 to 08/07/2013 and (b) 01/21/2014 to 01/26/2014.

the meteorological station can be influenced by the sea breeze in both directions (SW and SE) since differences in the SASA position and sea surface temperature can also influence the final direction result. During P1 (Fig. 6a), higher wind speed values (above 3.6 m s^{-1}) from the northeast were also identified, probably associated with the SASA position. For P2, when high concentrations of O_3 were recorded, the average wind speed between midnight and noon was below 2.04 m s^{-1} in all sites. Carvalho (2010) and da Silveira and Carvalho (2021) also identified a similar pattern. The analysis of the direction and wind speed at 10 m with the mixing ratio simulated by the WRF model also showed the sea breeze through most of the period (Fig. 7). In both study periods, the simulations depicted a similar configuration of the sea breeze during the afternoon. In the MARJ, the sea breeze is fundamental in the pollutant dispersion process (Carvalho, 2010; Pimentel et al., 2014; da Silveira and Carvalho, 2021), mainly in periods when the synoptic flow is weak, especially during the afternoons when wind speed is higher.

Figure 8a illustrates the influence of the sea breeze on PM_{10} concentrations at the Tijuca and Irajá stations, located in the central and northwestern regions of the MARJ, respectively. As highlighted by Pimentel et al. (2014), the sea breeze over the central region is mainly from the southeast, which may influence the transport of pollutants to the region's northwest (Carvalho, 2010; da Silveira and Carvalho, 2021). This can be verified on August 3, 2013, when (*i*) the highest concentrations of PM_{10} in Tijuca are recorded between 9:00 and 12:00 LT; (*ii*) the drop in concentrations at the station begins after 13:00 LT when it is possible to verify the breeze's entrance over the MARJ; (*iii*) there is an increase in PM_{10} concentrations in Irajá at 16:00 LT, when the breeze reaches the region. Carvalho (2010) also reported a similar pattern through numerical simulations with an air quality model for the MARJ.

Figure 8b also shows the influence of the sea breeze on O_3 concentrations at the São Cristóvão and Irajá stations, located in the central and northwestern regions of the MARJ, respectively. The wind direction data at São Cristóvão changed from east-northeast (between 7:00 and 11:00 LT) to south-southeast (between 12:00 and 20:00 LT). In Irajá, the sea breeze varies from southwest-west-northwest (between 10:00 and 13.00 LT) to south-southeast (14:00-17:00 LT). On January 22, 2014, the highest O_3 concentrations are recorded in São Cristovão between 10:00 and 15:00 LT, while the highest values in Irajá are recorded between 10:00 and 17:00 LT. These times are also identified as having the highest incidence of radiation, which demonstrates a typical behavior of O_3 formation. However, the action of the breezes

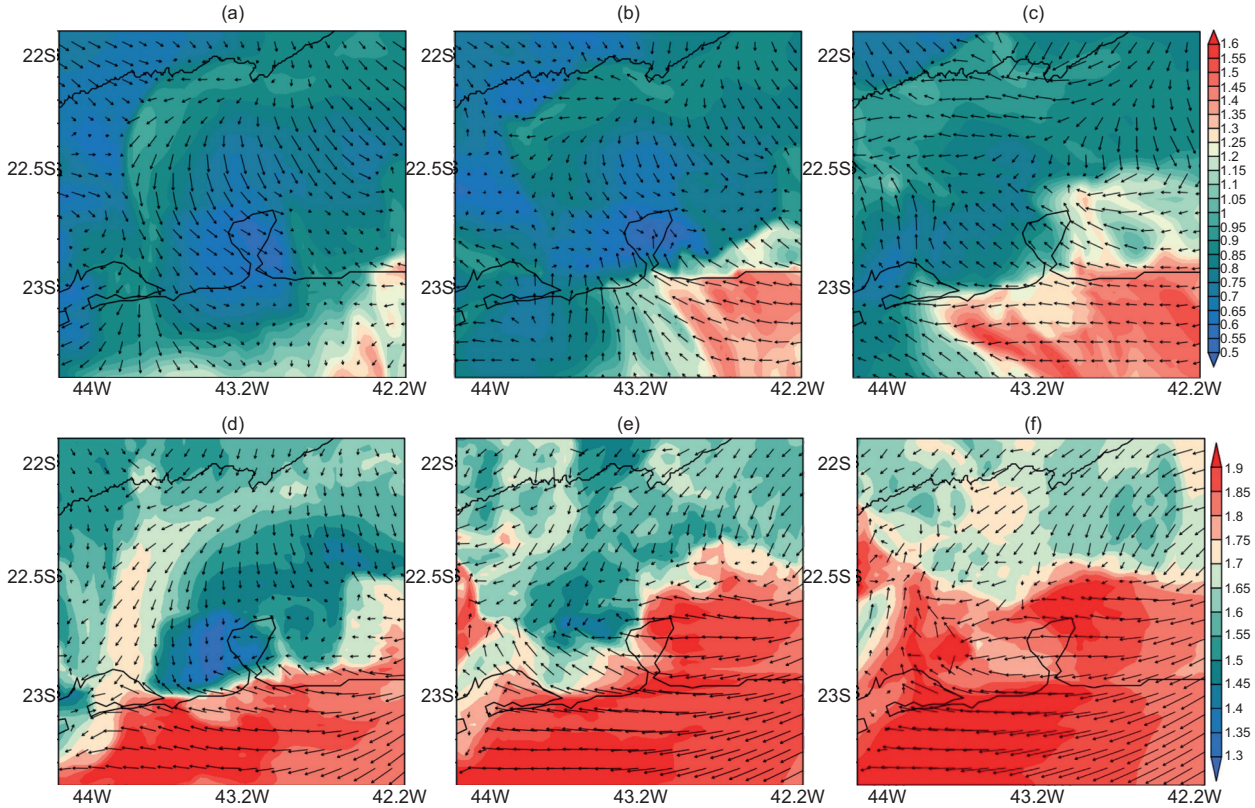

Fig. 7. WRF results for wind at 10 m (m s^{-1}) and mixing ratio (g kg^{-1}) on August 3, 2013 at (a) 15:00 UTC, (b) 18:00 UTC, (c) 21:00 UTC, and for January 23, 2014 at (d) 15:00 UTC, (e) 19:00 UTC, and (f) 21:00 through the 3-km grid (WRF).

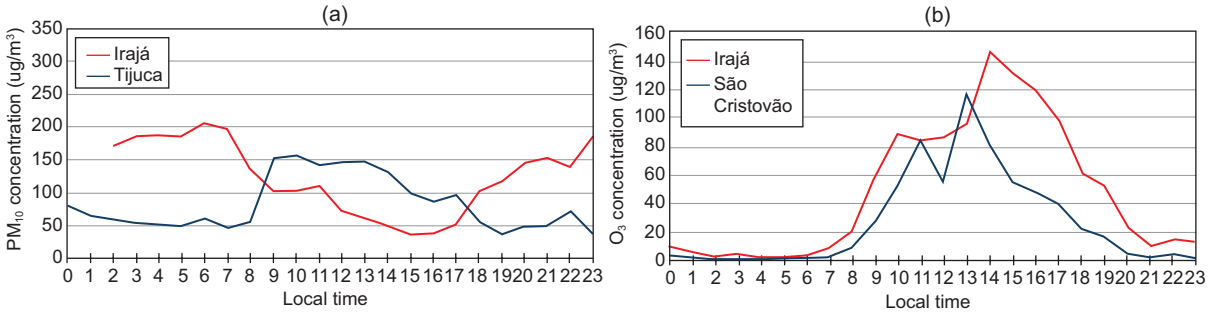

Fig. 8. Diurnal variations of concentrations of (a) PM_{10} on August 03, 2013 at Tijuca and Irajá stations and (b) O_3 on January 22, 2014 at São Cristovão and Irajá stations.

may indicate that pollutant transport to the northwest favors higher concentrations in Irajá (compared to São Cristovão). This can be supported by the analysis of the evolution of concentrations, which reveals that from 16:00 LT, the onset of a decrease in O_3 concentrations in São Cristovão is associated with an increase in concentrations in Irajá. It is worth mentioning that the São Cristovão station is located in an area with a high vehicular flow, which makes it difficult to draw definitive conclusions regarding

O_3, since the increase in vehicular flow in the late afternoon can also affect the VOC/NO_x ratios, in some cases favoring a decrease in O_3 concentrations. Therefore, it is possible to conclude that the sea breeze acts in the transport of pollutants from one region to another within the MARJ, leading to a subsequent decrease in pollutant concentrations in coastal regions and an increase in more distant regions, mainly in those located to the northwest. Although not clear in this study, the recirculation of pollutants due to the sea breeze circulation cell might also be an important feature in the maintenance of high pollutant concentration levels during multiple days, as shown by Grossi et al. (2000), Flocas et al. (2009), and Li et al. (2020).

3.2. PBL height and stability conditions

For both periods, the model simulated PBL height values were satisfactorily represented compared to observations, as shown in Figure 9, which reveals a good ability to predict the variable. The time evolution of the PBL diurnal cycle is also well captured by the model. Since the upper air data is measured at 12:00 and 00:00 UTC (~09:00 and 21:00 LT), it usually does not represent the maximum PBL height, which is found mostly in the late afternoon (Reuter, 2002). It is worth noting that the greatest differences (albeit small) were identified when the PBL height was below 100 m. A small delay in the model results when compared with observations is also clear. Several studies also indicated, based on sensitivity tests with numerical models, that the use of "non-local" PBL parameterizations, such as the YSU parameterization, produces results that are more consistent with observations (Xie et al., 2012; Wang et al., 2014; Banks and Baldasano, 2016; Banks et al., 2016).

The Richardson number and the classification proposed by Clifton et al. (2013) were used to define the atmospheric stability from observations and modeled

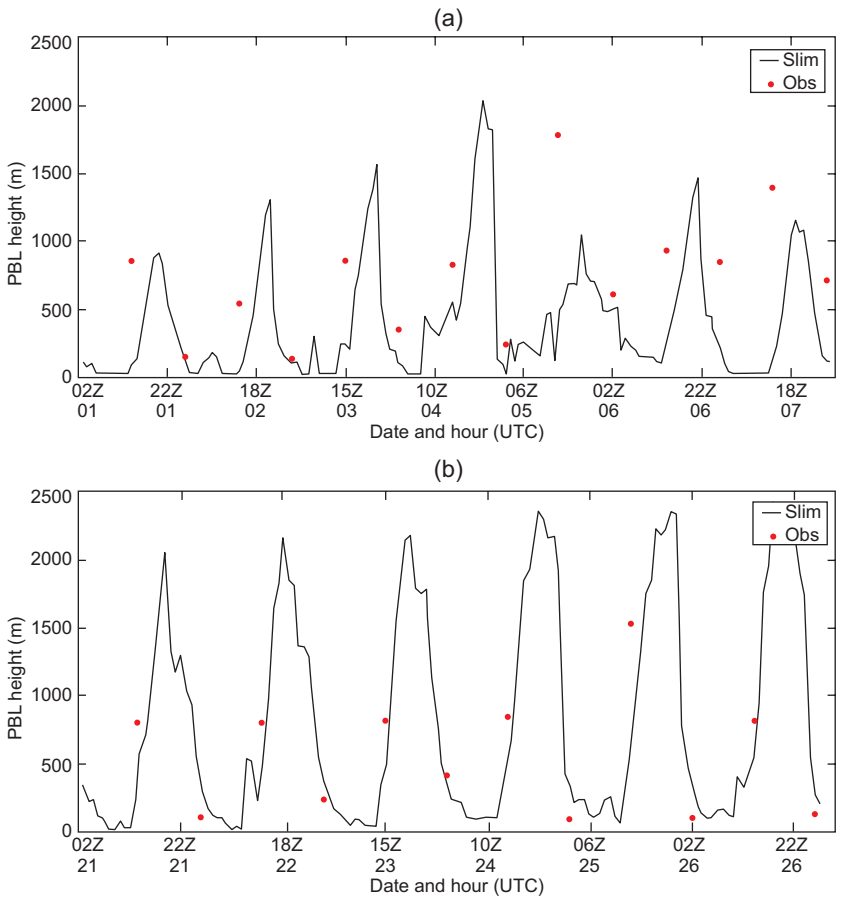

Fig. 9. Height (m) of simulated and observed PBL at Galeão Airport (SBGL) for the period between (a) August 1 and 7, 2013 and (b) January 21 and 26, 2014.

data in the study periods. The comparison considered the data simulated by the WRF model on the 3-km grid for the grid point closest to the Galeão International Airport and the data obtained from radiosondes. For P1 (Table IV) at 12:00 and 00:00 UTC, there is an agreement between the model and observations in 70% of the days. Despite representing the PBL height satisfactorily at most times, the model had difficulty simulating the conditions of a neutral atmosphere. As for P2 (Table V), the comparison between observed and simulated data showed agreement in atmospheric stability in 66% (33%) of the days at 12:00 (00:00) UTC (Table V).

During the summer, the model revealed a lower skill in representing nighttime stability, which may be associated with the difficulty of the model in estimating the nocturnal cooling of the surface and lower atmosphere levels. The underestimation of the diurnal cycle amplitude by weather models can be a response to a misrepresentation of the soil properties and land use characteristics (Ács et al., 2014) and/or of an air mass advection (de Bode et al., 2021).

Figure 10 presents the vertical profile of the potential and dew point temperatures from simulations and observations during a specific time and date, chosen according to the availability of observations. The vertical potential temperature profile is generally well represented, with slightly higher differences in the layer below 800 hPa. Models have lower performance in simulating the atmospheric variables in the layers closest to the surface due to the difficulty in representing the mixture in the vertical layer, mainly

Table IV. Observed and simulated atmospheric stability conditions from 08/01/2013 to 08/07/2013 at the Galeão Airport (SBGL).

	Stability			
	09:00 LT (12:00 UTC)		21:00 LT (00:00 UTC)	
Date (September)	Observed	Simulated	Observed	Simulated
1	Stable	Stable	Stable	Stable
2	Unstable	Stable	Stable	Stable
3	Stable	Stable	Stable	Stable
4	Neutral	Unstable	Stable	Stable
5	Unstable	Unstable	Neutral	Unstable
6	Unstable	Unstable	Neutral	Stable
7	Unstable	Unstable	Stable	Stable

Table V. Observed and simulated atmospheric stability conditions from 01/21/2014 to 01/26/2014 at the Galeão Airport (SBGL).

	Stability			
	10:00 LT (12:00 UTC)		22:00 LT (00:00)	
Date (January)	Observed	Simulated	Observed	Simulated
21	Unstable	Unstable	Stable	Stable
22	Unstable	Unstable	Stable	Unstable
23	Unstable	Unstable	Stable	Neutral
24	Unstable	Neutral	Stable	Neutral
25	Unstable	Neutral	Stable	Stable
26	Unstable	Unstable	Neutral	Stable

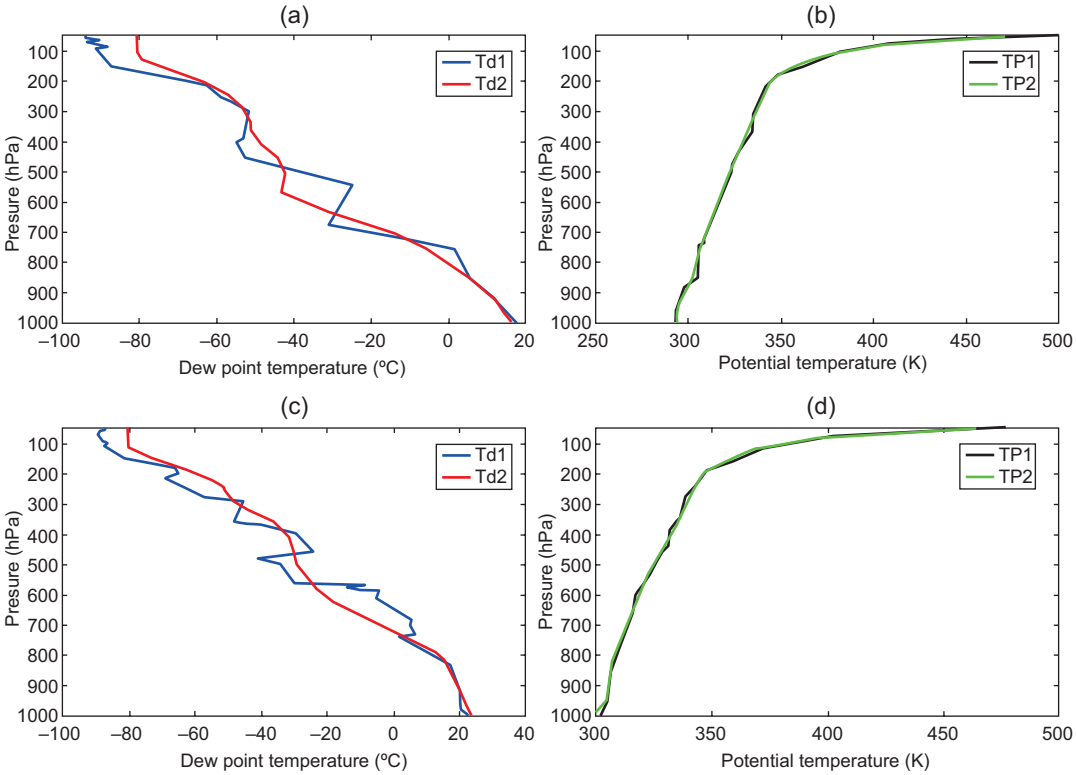

Fig. 10. Simulated and observed vertical profile of (a) dew point temperature and (b) potential temperature on 08/06/2013 at 12:00 UTC; and (c) dew point temperature and (d) potential temperature on 01/22/2014 at 00:00 UTC. (Td1: observed Td, in blue; Td2: simulated Td, in red; TP1: observed θ, in black; and TP2: simulated θ, in green).

due to the complex terrain and land use representation (Hu et al., 2013). The WRF has low skill in simulating the dew point temperature (Fig. 10), which can be associated with several factors: use of climatological sea surface temperature, misrepresentation of land use and terrain details, high urbanization and the presence of large bodies of water, and large vegetated areas of our study area. For P1, the temperature and dew point temperature behavior analysis indicated that the model represented wet and dry layers well. For P2, it is observed that the model had greater difficulty in representing the wet layers.

3.3 Atmospheric stability vs. pollutant concentration

To evaluate the impact of atmospheric stability on the PM_{10} concentration, the results of the meteorological station of Pedra de Guaratiba will be presented as an example. Figure 11 shows the evolution of PM_{10} concentrations recorded at this station and the stability classification estimated from the results of the WRF model during P1. The results revealed stable atmospheric conditions in 67% of the cases, unstable conditions in 26%, and neutral conditions in 6%. This agrees with what is typically observed during the winter in the region when the atmosphere is more conducive to stability conditions due to a lower incidence of solar radiation and SASA performance (Santos et al., 2016; Reboita et al., 2019). The highest concentrations of PM_{10} occur in the first four days when there is a stable atmosphere during most hours, which is less conducive to the dispersion of pollutants. The lowest concentrations were verified on days 5 and 6 when P1 presented unstable conditions during subsequent times. The times of decrease in concentration on all days also agree with the time when the sea breeze reaches the region. Lower concentrations are also associated with higher PBL heights, and high concentrations are associated with lower PBL heights.

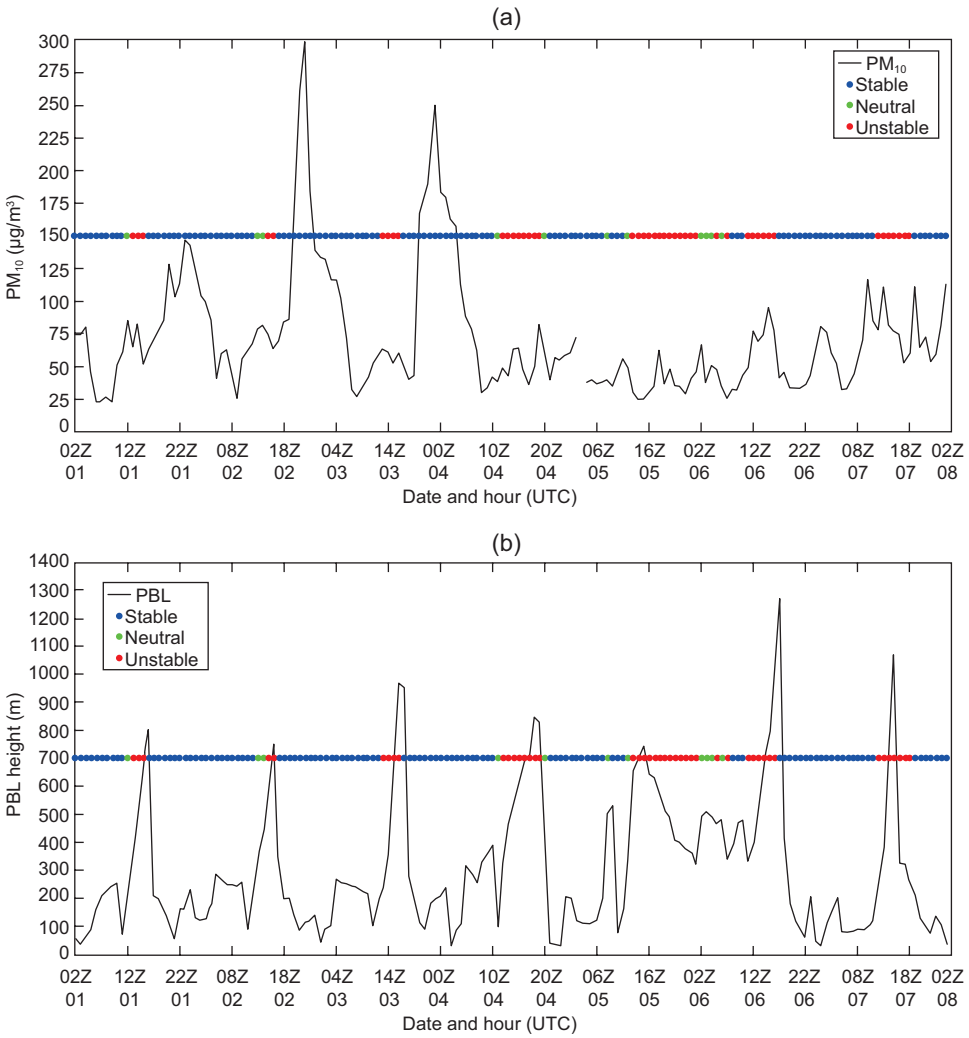

Fig. 11. (a) Stability and concentration of PM_{10} during the period from 08/01/2013 to 08/07/2013; (b) stability and height of the PBL during the period from 08/01/2013 to 08/07/2013 at Pedra de Guaratiba station.

Figure 12 shows the evolution of O_3 concentrations and the atmospheric stability classification at Pedra Guaratiba station during P2. The model results reveal stable atmospheric conditions in 65% of the cases, neutral conditions in 21%, and unstable conditions in 14%. This behavior is atypical for a summer period when the atmosphere presents a period of greater instability, especially during the afternoon due to the intense heating of the surface. The highest ozone peaks occurred around 15:00 LT when the greatest radiation incidence occurred. Most of the time, the model simulates the transition from an unstable atmosphere to a stable one (also reported by Herrera-Mejía and Hoyos, 2019). The predominance of stable conditions during the summer, when high O_3 concentrations were registered, may represent a significant association. It is noteworthy that since the formation of O_3 requires the incidence of solar radiation, the dependence on stability conditions is often not studied.

4. Conclusions

This study aimed to evaluate the PBL conditions simulated by the WRF model and its impact on air quality during days when episodes of high

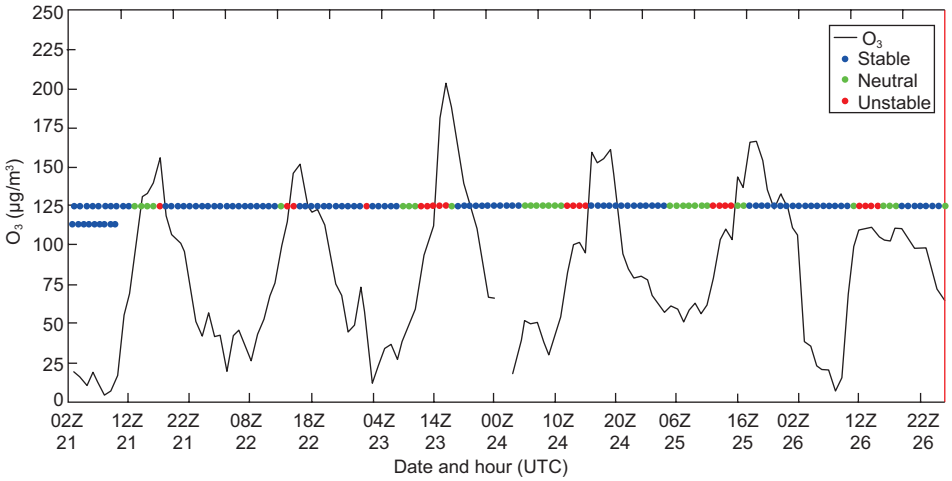

Fig. 12. Atmospheric stability estimated with WRF (color points) and O_3 concentrations measured at Pedra de Guaratiba (black line) between 21/01/2014 and 26/01/2014.

concentrations of O_3 and PM_{10} were recorded in the MARJ. The influence of SASA in both periods was verified. Under the influence of the SASA, the southeast region predominantly presents clear sky conditions and light winds, which favors the maintenance of episodes with high pollutants concentration in the region. It should be noted that despite different formation mechanisms, periods with high concentrations of O_3 and PM_{10} presented similar meteorological conditions regarding the mean sea level pressure, cloud cover, and winds conditions. All of these conditions were represented satisfactorily by the WRF results. The analysis of the model results and the observations allowed the identification of the sea breeze and the impact on the transport of pollutants from coastal areas to regions further away from the coast (predominantly located in the northeast/northwest direction).

Verification of the vertical profile of potential temperature showed agreement between the results simulated by the WRF and the observations. The comparison of the classification between the atmospheric stability, verified through the Ri number from upper-air observations and WRF results, showed a greater agreement during the day in the summer and at night during winter. The comparison between the PBL height obtained through observations and the model results revealed adequate results. Thus, the results obtained in this study can support the use of PBL height data generated by meteorological models in regulatory air quality models that require such information. However, further studies are needed to expand the verification of the WRF model performance and of other meteorological models for other meteorological situations and regions of Brazil.

The evaluation of the impact of stability revealed that the highest concentrations of PM_{10} were verified in times of stable atmosphere and with low PBL height. The highest concentrations of O_3 occurred during times of atmospheric instability, which coincide with those with the highest incidence of solar radiation; however, the results indicate that stability conditions may be conducive to maintaining the pollutant over the region. In this context, based on the assessment of the high dependence of pollutants on meteorological conditions, it is possible to conclude that meteorological forecasting, combined with knowledge about the emission sources of priority pollutants and the topography of a region, can be used as an indication for the air quality forecast in a region.

Acknowledgment

This work was supported by the Conselho Nacional de Desenvolvimento Científico e Tecnológico (National Council for Scientific and Technological Development, CNPq) and by the Coordenação de Aperfeiçoamento de Pessoal de Nível Superior (Coordination for the Improvement of Higher Education Personnel, CAPES).

References

Ács F, Gyöngyösi AZ, Breuer H, Horváth Á, Mona T, Rajkai K. 2014. Sensitivity of WRF-simulated planetary boundary layer height to land cover and soil changes. Meteorologische Zeitschrift 23: 279-293. https://doi.org/10.1127/0941-2948/2014/0544

Baklanov A, Molina LT, Gauss M. 2016. Megacities, air quality and climate. Atmospheric Environment 126: 235-249. https://doi.org/10.1016/j.atmosenv.2015.11.059

Banks RF, Baldasano JM. 2016. Impact of WRF model PBL schemes on air quality simulations over Catalonia, Spain. Science of The Total Environment 572: 98-113. https://doi.org/10.1016/j.scitotenv.2016.07.167

Banks RF, Tiana-Alsina J, Baldasano JM, Rocadenbosch F, Papayannis A, Solomos S, Tzanis CG. 2016. Sensitivity of boundary-layer variables to PBL schemes in the WRF model based on surface meteorological observations, lidar, and radiosondes during the HygrA-CD campaign. Atmospheric Research 176-177: 185-201. https://doi.org/10.1016/j.atmosres.2016.02.024

Beringui K, Justo EPS, Ventura LMB, Gomes RGS, Lionel-Mateus V, de la Cruz AH, de Almeida ACLB, Ramos MB, Suazo JA, Valle PHR, Gioda A. 2023. The contribution of meteorological parameters and the COVID-19 partial lockdown on air quality in Rio de Janeiro, Brazil. Journal of the Brazilian Chemical Society 34: 69-82. https://doi.org/10.21577/0103-5053.20220089

Bodor K, Szép R, Bodor, Z. 2022. Time series analysis of the air pollution around Ploiesti oil refining complex, one of the most polluted regions in Romania. Scientific Reports 12: 11817. https://doi.org/10.1038/s41598-022-16015-7

Carvalho VSB. 2010. O impacto das megacidades sobre a qualidade do ar: os casos das regiões metropolitanas de São Paulo e do Rio de Janeiro. Ph.D. thesis, Instituto de Astronomia, Geofísica e Ciências Atmosféricas, Universidade de São Paulo.

Carvalho VSB, de Freitas ED, Mazzoli CR, Andrade MF. 2012. Avaliação da influência de condições meteorológicas na ocorrência e manutenção de um episódio prolongado com altas concentrações de ozônio sobre a Região Metropolitana de São Paulo. Revista Brasileira de Meteorologia 27: 463-474. https://doi.org/10.1590/S0102-77862012000400009

Carvalho VSB, Freitas ED, Martins LD, Martins JA, Mazzoli CR, Andrade MF. 2015. Air quality status and trends over the Metropolitan Area of São Paulo, Brazil as a result of emission control policies. Environmental Science & Policy 47: 68-79. https://doi.org/10.1016/j.envsci.2014.11.001

Carvalho H. 2021. New WHO global air quality guidelines: More pressure on nations to reduce air pollution levels. The Lancet Planetary Health 5: e760-e761. https://doi.org/10.1016/S2542-5196(21)00287-4

Cavalcanti PMPS. 2003. Avaliação dos impactos causados na qualidade do ar pela geração termelétrica. M.Sc. thesis, Universidade Federal do Rio de Janeiro.

Chen SH, Sun WY. 2002. A one-dimensional time dependent cloud model. Journal of the Meteorological Society of Japan. Series II 80: 99-118. https://doi.org/10.2151/jmsj.80.99

Clifton A, Schreck S, Scott G, Kelley N, Lundquist JK. 2013. Turbine inflow characterization at the National Wind Technology Center. Journal of Solar Energy Engineering 135: 031017. https://doi.org/10.1115/1.4024068

CONAMA. 2018. Resolução n. 491, de 19 de novembro de 2018. Dispõe sobre padrões de qualidade do ar. Ministério do Meio Ambiente/Conselho Nacional do Meio Ambiente. Diário oficial da República Federativa do Brasil, Brasília, 19 de novembro.

Crawford J, Chambers S, Cohen D, Williams A, Griffiths A, Stelcer E. 2016. Assessing the impact of atmospheric stability on locally and remotely sourced aerosols at Richmond, Australia, using Radon-222. Atmospheric Environment 127: 107-117. https://doi.org/10.1016/j.atmosenv.2015.12.034

Dantas G, Siciliano B, França BB, da Silva CM, Arbilla G. 2020. The impact of COVID-19 partial lockdown on the air quality of the city of Rio de Janeiro, Brazil. Science of The Total Environment 729: 139085. https://doi.org/10.1016/j.scitotenv.2020.139085

Da Silva Júnior RS Andrade MdF. 2013. Validação de poluentes fotoquímicos e inclusão do inventário de emissões no modelo de qualidade do ar WRF/CHEM, para a região metropolitana de São Paulo. Revista Brasileira de Meteorologia 28: 105-121. https://doi.org/10.1590/S0102-77862013000100010

Da Silveira WW, Carvalho VSB. 2021. Avaliação das Condições Meteorológicas Simuladas pelo Modelo WRF na Região Metropolitana do Rio de Janeiro em Dias Com Altas Concentrações de Poluentes. Revista Brasileira de Meteorologia 36: 317-325. https://doi.org/10.1590/0102-77863620067

De Bode M, Hedde T, Roubin P, Durand P. 2021. Fine-resolution WRF simulation of stably stratified flows in shallow pre-alpine valleys: A case study of the KASCADE-2017 campaign. Atmosphere 12: 1063. https://doi.org/10.3390/atmos12081063

DECEA. 2023. Como decodificar o METAR e o SPECI? Departamento de Controle do Espaço Aéreo. Available at https://ajuda.decea.mil.br/base-de-conhecimento/como-decodificar-o-metar-e-o-speci/ (accessed 2023 August 17)

Dereczynski CP, de Oliveira JS, Machado CO. 2009. Climatologia da precipitação no município do Rio de Janeiro. Revista Brasileira de Meteorologia 24: 24-38. https://doi.org/10.1590/S0102-77862009000100003

Dudhia J. 1989. Numerical study of convection observed during the winter monsoon experiment using a mesoscale two-dimensional model. Journal of Atmospheric Sciences 46: 3077-3107. https://doi.org/10.1175/1520-0469(1989)046<3077:NSOCOD>2.0.CO;2

Ferreira GWS, Reboita MS. 2022. A new look into the South America precipitation regimes: Observation and forecast. Atmosphere 13: 873. https://doi.org/10.3390/atmos13060873

Flocas H, Kelessis A, Helmis C, Petrakakis M, Zoumakis M, Pappas K. 2009. Synoptic and local scale atmospheric circulation associated with air pollution episodes in an urban Mediterranean area. Theoretical and Applied Climatology 95: 265-277. https://doi.org/10.1007/s00704-008-0005-9

Geraldino CGP, Martins EM, da Silva CM, Arbilla G. 2017. An analytical investigation of ozone episodes in Bangu, Rio de Janeiro. Bulletin of Environmental Contamination and Toxicology 98: 632-637. https://doi.org/10.1007/s00128-017-2041-6

Gómez-Peláez LM, Santos JM, de Almeida Albuquerque TT, Reis Jr NC, Andreão WL, de Fátima Andrade M. 2020. Air quality status and trends over large cities in South America. Environmental Science & Policy 114: 422-435. https://doi.org/10.1016/j.envsci.2020.09.009

Grossi P, Thunis P, Martilli A, Clappier A. 2000. Effect of sea breeze on air pollution in the greater Athens area. Part II: Analysis of different emission scenarios. Journal of Applied Meteorology and Climatology 39: 563-575. https://doi.org/10.1175/1520-0450(2000)039<0563:EOSBOA>2.0.CO;2

Herrera-Mejía L, Hoyos CD. 2019. Characterization of the atmospheric boundary layer in a narrow tropical valley using remote-sensing and radiosonde observations and the WRF model: the Aburrá Valley case-study. Quarterly Journal of the Royal Meteorological Society 145: 2641-2665. https://doi.org/10.1002/qj.3583

Hong SY, Noh Y, Dudhia J. 2006. A new vertical diffusion package with an explicit treatment of entrainment processes. Monthly Weather Review 134: 2318-2341. https://doi.org/10.1175/MWR3199.1

Hu XM, Klein PM, Xue M. 2013. Evaluation of the updated YSU planetary boundary layer scheme within WRF for wind resource and air quality assessments. Journal of Geophysical Research: Atmospheres 118: 10490-10505. https://doi.org/10.1002/jgrd.50823

INEA. 2020. Relatório da qualidade do ar do Estado do Rio de Janeiro: ano base 2018. Instituto Estadual do Ambiente, Rio de Janeiro.

Janjić ZI. 2001. Nonsingular implementation of the Mellor-Yamada level 2.5 scheme in the NCEP Meso model. Office note 437. National Centers for Environmental Prediction. Available at https://repository.library.noaa.gov/view/noaa/11409 (accessed 2023 August 17)

Kain JS. 2004. The Kain-Fritsch convective parameterization: An update. Journal of Applied Meteorology and Climatology 43: 170-181. https://doi.org/10.1175/1520-0450(2004)043<0170:TKCPAU>2.0.CO;2

Li X, Hu XM, Ma Y, Wang Y, Li L, Zhao Z. 2019. Impact of planetary boundary layer structure on the formation and evolution of air-pollution episodes in Shenyang, Northeast China. Atmospheric Environment 214: 116850. https://doi.org/10.1016/j.atmosenv.2019.116850

Li W, Wang Y, Bernier C, Estes M. 2020. Identification of sea breeze recirculation and its effects on ozone in Houston, TX, during DISCOVER-AQ 2013. Journal of Geophysical Research: Atmospheres 125: e2020JD033165. https://doi.org/10.1029/2020JD033165

Mello R. 2017. Análise da representatividade locacional de uma estação de monitoramento da qualidade do ar a partir da utilização de amostradores passivos. M.Sc. thesis, Universidade Federal do Rio de Janeiro.

Mendes D, Dantas G, da Silva MA, de Seixas EG, da Silva CM, Arbilla G. 2020. Impact of the Petrochemical Complex on the Air Quality of an Urban Area in the City of Rio de Janeiro, Brazil. Bulletin of Environmental Contamination and Toxicology 104: 438-443. https://doi.org/10.1007/s00128-020-02802-3

Miao Y, Li J, Miao S, Che H, Wang Y, Zhang X, Zhu R, Liu S. 2019. Interaction between planetary boundary

layer and PM 2.5 pollution in megacities in China: A review. Current Pollution Reports 5: 261-271. https://doi.org/10.1007/s40726-019-00124-5

Mlawer EJ, Taubman SJ, Brown PD, Iacono MJ, Clough SA. 1997. Radiative transfer for inhomogeneous atmospheres: RRTM, a validated correlated-k model for the longwave. Journal of Geophysical Research: Atmospheres 102: 16663-16682. https://doi.org/10.1029/97JD00237

Mohan M, Siddiqui TA. 1998. Analysis of various schemes for the estimation of atmospheric stability classification. Atmospheric Environment 32: 3775-3781. https://doi.org/10.1016/S1352-2310(98)00109-5

Molina LT. 2021. Introductory lecture: Air quality in megacities. Faraday Discussions 226: 9-52. https://doi.org/10.1039/D0FD00123F

Moura PH, Santos DWL, Moreno AM, Sobreira PGP, Silva FP, Maia LFPG. 2020. Análise da qualidade do ar e fatores meteorológicos na cidade de Nova Iguaçu (Rio de Janeiro-Brasil) entre os anos de 2000 a 2016. Revista Brasileira de Meio Ambiente 8: 87-99. https://doi.org/10.5281/zenodo.3633889

Muramatsu S, McGee TG, Mori K. 2021. Living in the megacity: Towards sustainable urban environments. Springer Japan, Tokyo.

Pimentel LCG, Correia EB, Marton E, Cataldi M, Nogueira E. 2014. Influência dos parâmetros de configuração do modelo CALMET sobre a simulação da circulação atmosférica na região metropolitana do Rio de Janeiro. Revista Brasileira de Meteorologia 29: 579-596. https://doi.org/10.1590/0102-778620130099

Reboita MS, Gan MA, da Rocha RP, Ambrizzi T. 2010. Regimes de precipitação na América do Sul: uma revisão bibliográfica. Revista Brasileira de Meteorologia 25: 185-204. https://doi.org/10.1590/S0102-77862010000200004

Reboita MS, Ambrizzi T, Silva BA, Pinheiro RF, da Rocha RP. 2019. The South Atlantic subtropical anticyclone: Present and future climate. Frontiers in Earth Science 7: 8. https://doi.org/10.3389/feart.2019.00008

Reuter EDJ. 2002. Estudo das camadas limites planetária marinha e continental na região do Centro de Lançamento de Alcântara. M.Sc. thesis, Instituto Nacional de Pesquisas Espaciais.

Sánchez MP. 2017. Investigação da camada limite urbana na região metropolitana de São Paulo. M.Sc. thesis, Universidade de São Paulo.

Santos TC, Carvalho VSB, Reboita MS. 2016. Avaliação da influência das condições meteorológicas em dias com altas concentrações de material particulado na Região Metropolitana do Rio de Janeiro. Engenharia Sanitária e Ambiental 21: 307-313. https://doi.org/10.1590/S1413-41522016139269

Santos EM, Azevedo DdA. 2021. Impact on ground-level ozone formation by emission characterization of volatile organic compounds from a flex-fuel light-duty vehicle fleet in a traffic tunnel in Rio de Janeiro, Brazil. Air Quality, Atmosphere & Health 14: 259-270. https://doi.org/10.1007/s11869-020-00931-6

Schüch D, de Freitas ED, Espinosa SI, Martins LD, Carvalho VSB, Ramin BF, Silva JS, Martins JA, de Fatima Andrade M. 2019. A two decades study on ozone variability and trend over the main urban areas of the São Paulo state, Brazil. Environmental Science and Pollution Research 26: 31699-31716. https://doi.org/10.1007/s11356-019-06200-z

Skamarock WC, Klemp JB, Dudhia J, Gill DO, Barker D, Duda MG, Huang XY, Wang W, Powers JG. 2008. A Description of the Advanced Research WRF Version 3 (No. NCAR/TN-475+STR). University Corporation for Atmospheric Research. doi:10.5065/D68S4MVH

Stull RB. 1991. An Introduction to Boundary Layer Meteorology. Kluwer Academic Publishers, Dordrecht.

Trindade HA, Oliveira AE, Pfeiffer WC, Londres H, Costa-Ribeiro C. 1980. Meteorological parameters and concentration of total suspended particulates in the urban area of Rio de Janeiro. Atmospheric Environment (1967) 14: 973-978. https://doi.org/10.1016/0004-6981(80)90012-8

Tsuruta F, de Carvalho NJ, da Silva CM, Arbilla G. 2018. Air quality indexes in the city of Rio de Janeiro during the 2016 Olympic and Paralympic Games. Journal of the Brazilian Chemical Society 29: 1291-1303. https://doi.org/10.21577/0103-5053.20170226

UN. 2019. World urbanization prospects: The 2018 revision (ST/ESA/SER.A/420). United Nations, Department of Economic and Social Affairs, Population Division, United Nations, New York.

UN. 2022. The sustainable development goals: Report 2022. United Nations, New York.

UN-HABITAT. 2022. World cities report 2022: Envisaging the future of cities. United Nations Human Settlements Programme, Nairobi, Kenya, 41-44.

Wang ZQ, Duan AM, Wu GZ. 2014. Impacts of boundary layer parameterization schemes and air-sea coupling on WRF simulation of the East Asian summer monsoon.

Science China Earth Sciences 57: 1480-1493. https://doi.org/10.1007/s11430-013-4801-4

Wang F, Chambers SD, Zhang Z, Williams AG, Deng X, Zhang H, Lonati G, Crawford J, Griffiths AD, Ianniello A, Allegrini I. 2016. Quantifying stability influences on air pollution in Lanzhou, China, using a radon-based "stability monitor": Seasonality and extreme events. Atmospheric Environment 145: 376-391. https://doi.org/10.1016/j.atmosenv.2016.09.014

WHO. 2005. WHO global air quality guidelines: Particulate matter, ozone, nitrogen dioxide and sulfur dioxide. Global Update 2005. World Health Organization, Regional Office for Europe, Copenhagen, Denmark.

WHO. 2021. WHO global air quality guidelines. Particulate Matter ($PM_{2.5}$ and PM_{10}), Ozone, Nitrogen Dioxide, Sulfur Dioxide and Carbon Monoxide. Executive summary. World Health Organization, Geneva.

Xie B, Fung JCH, Chan A, Lau A. 2012. Evaluation of nonlocal and local planetary boundary layer schemes in the WRF model. Journal of Geophysical Research: Atmospheres 117: D12103. https://doi.org/10.1029/2011JD017080

Zhang Z, Wang F, Costabile F, Allegrini I, Liu F, Hong W. 2012. Interpretation of ground-level ozone episodes with atmospheric stability index measurement. Environmental Science and Pollution Research 19: 3421-3429. https://doi.org/10.1007/s11356-012-0867-3